

A new probe of magnetic fields during high-mass star formation

Zeeman splitting of 6.7 GHz methanol masers

W.H.T. Vlemmings¹

Argelander Institute for Astronomy, University of Bonn, Auf dem Hügel 71, 53121 Bonn, Germany

Received ; accepted

ABSTRACT

Context. The role of magnetic fields during high-mass star formation is a matter of fierce debate, yet only a few direct probes of magnetic field strengths are available.

Aims. The magnetic field is detected in a number of massive star-forming regions through polarization observations of 6.7 GHz methanol masers. Although these masers are the most abundant of the maser species occurring during high-mass star formation, most magnetic field measurements in the high-density gas currently come from OH and H₂O maser observations.

Methods. The 100-m Effelsberg telescope was used to measure the Zeeman splitting of 6.7 GHz methanol masers for the first time. The observations were performed on a sample of 24 bright northern maser sources.

Results. Significant Zeeman splitting is detected in 17 of the sources with an average magnitude of 0.56 m s⁻¹. Using the current best estimate of the 6.7 GHz methanol maser Zeeman splitting coefficient and a geometrical correction, this corresponds to an absolute magnetic field strength of 23 mG in the methanol maser region.

Conclusions. The magnetic field is dynamically important in the dense maser regions. No clear relation is found with the available OH maser magnetic field measurements. The general sense of direction of the magnetic field is consistent with other Galactic magnetic field measurements, although a few of the masers display a change of direction between different maser features. Due to the abundance of methanol masers, measuring their Zeeman splitting provides the opportunity to construct a comprehensive sample of magnetic fields in high-mass star-forming regions.

Key words. masers – polarization – Stars: formation – magnetic fields

1. Introduction

Although massive stars play an important role in the chemical and energetic evolution of their host galaxies, their formation mechanism remains elusive. This problem is the topic of extensive observational and theoretical efforts. Even though few of the current simulations include magnetic fields, the influence of magnetism on the star formation processes is extensive as it can support a molecular cloud against collapse, affect core fragmentation and change the feedback processes (e.g. Krumholz & Bonnell, 2007, and references therein).

Most current high-mass star formation magnetic field information comes from H₂O and OH maser polarization observations. The observations of the H₂O maser Zeeman effect using Very Long Baseline Interferometry (VLBI) reveal field strengths between 10 and 600 mG, while the linear polarization measurements reveal a complex but often ordered magnetic field morphology (e.g. Vlemmings et al., 2006a). Aside from H₂O masers, tracing high-density regions ($n_{\text{H}_2} \approx 10^8 - 10^{11} \text{ cm}^{-3}$), the magnetic field in the less dense surrounding regions is typically probed by polarimetric OH maser observations (e.g. Bartkiewicz et al., 2005). These observations reveal fields of a few mG as well as ordered structure in the magnetic field. However, the strongest and most abundant of the high-mass star formation region masers arises from the 6.7 GHz $5_1 - 6_0A^+$ methanol transition, and for this maser hitherto only very few polarization observations exist.

Over 95% of the class II 6.7 GHz masers have been found to harbor warm dust emission, even though only some of the masers are associated with a detectable ultra-compact (UC) HII region (e.g. Hill et al., 2005). This seems to indicate that the masers probe a range of early phases of massive star formation. The 6.7 GHz masers are likely pumped by a combination of collisions and emission from nearby, warm ($T > 150 \text{ K}$) dust, but themselves arise from gas at much lower temperature ($T < 50 \text{ K}$) with high hydrogen number densities ($n_{\text{H}_2} > 10^6 \text{ cm}^{-3}$) and a high methanol abundance (e.g. Sobolev et al., 1997; Cragg et al., 2005). Like H₂O, methanol is a non-paramagnetic molecule, and thus both the linear and circular polarization fractions are small. The first polarization measurements were made with the Australia Telescope Compact Array (ATCA) on the 6.7 GHz maser toward a handful of southern massive star-forming regions (Ellingsen, 2002) and linear polarization between few and 10% was detected. The first high angular resolution linear polarization maps were recently made using MERLIN (Vlemmings et al., 2006b) and the Long Baseline Array (Dodson 2008). These observations indicate a typical linear polarization fraction of $\sim 2 - 3\%$. In addition to the first linear polarization measurements, a marginal possible detection of circular polarization, caused by the Zeeman effect, was made for the masers of the ON1 starforming region (Green et al., 2007).

This paper presents the first significant detection of Zeeman splitting in the 6.7 GHz maser transition for a sample of northern massive star-forming regions. The observations, data reduction and error analysis are discussed in § 2 and methanol maser

Zeeman splitting in § 3. The results are given in § 4 and are discussed in § 5.

2. Observations & analysis

2.1. Effelsberg observations & data reduction

The 6668.512 MHz ($5_1 - 6_0A^+$) methanol maser line of a sample of massive star-forming regions was observed on Nov 12th 2007 using the 5 cm primary focus receiver of the 100-m Effelsberg¹ telescope. The data were taken in position switch mode with a 2 minute cycle time. The full width at half-maximum (FWHM) beam of the telescope is $\sim 120''$ at the maser frequency. Data were collected using the fast Fourier transform spectrometer (FFTS) using two spectral windows, corresponding to the right- and left-circular polarizations (RCP and LCP). The spectral windows of 20 MHz were divided in 16384 spectral channels, resulting in a $\sim 0.055 \text{ km s}^{-1}$ channel spacing and were centered on the local standard of rest (LSR) source velocities.

The data were reduced using the Continuum and Line Analysis Single-dish Software (CLASS) package. The amplitudes were calibrated using scans on 3C123, 3C286 and 3C84. No special efforts were undertaken to model short time-scale gain fluctuations during the observations, however, the small gain difference between the RCP and LCP was corrected. Small RCP and LCP gain differences do not affect the Zeeman splitting determination when using the cross correlation method, as with this method the Zeeman splitting measurements are not reliant on accurate absolute fluxes. It is found that in general the measured peak fluxes agree well with the literature values in the methanol maser catalogue of Pestalozzi et al. (2005). From the literature comparison and from a comparison of the measured flux of G9.62+0.20, which is the target of regular monitoring, with the flux obtained on Nov 12th with the Hartebeesthoek radio telescope (S. Goedhart, priv. communication), the absolute flux errors are estimated to be $\sim 10\%$. Still, for a few sources the measured flux density is up to 50% different from the published values, which is likely due to variability and/or structural changes in the maser themselves.

2.2. The source sample

The sample was taken from the 6.7 GHz methanol maser catalogue by Pestalozzi et al. (2005) and consists of some of the strongest ($> 50 \text{ Jy}$) northern maser sources observable from Effelsberg. Priority was given to sources previously observed at high resolution or with existing OH/H₂O maser polarization observations. To detect the Zeeman splitting the goal was to reach a signal-to-noise of > 3000 and thus the total integration time per source was variable. As the observations were limited to 13 hours, source selection also depended on observability and was occasionally adjusted based on the flux detected in a first observing scan. As a result, the noise level is different for each of the sources and ranges from 20 mJy to 100 mJy for each polarization.

2.3. Zeeman splitting determination

The circular polarization fraction arising from the small Zeeman splitting of the paramagnetic methanol molecule, is extremely

low ($< 0.5\%$). Detection of such small circular polarization fraction is very sensitive to an accurate relative calibration between the RCP and LCP signals. Zeeman splitting can be detected relatively straightforward using the cross-correlation method, described by Modjaz et al. (2005). This method directly determines the Zeeman splitting from the RCP and LCP data. It has been shown to be robust against the relative RCP and LCP gain calibration errors while still reaching a comparable sensitivity as performing S-curve fitting to the circular polarization spectrum. Also, essential for single dish work, it is able to measure Zeeman splitting in the case of spectrally blended maser features in a straightforward manner without the need for fitting a number of Gaussian components to identify individual maser features. It was for instance used on Green Bank Telescope data to determine limits on the Zeeman splitting for two H₂O maser megamasers galaxies (Modjaz et al., 2005; Vlemmings et al., 2007).

As many of the sources will have blended maser features, and to reduce the effect of remaining RCP and LCP gain calibration errors, the Zeeman splitting is thus determined using the cross-correlation method. Applying this method to the entire maser spectrum essentially means that the resulting Zeeman splitting is a flux weighted average of the true Zeeman splitting. To examine changes of the magnetic field over the maser spectrum, one can perform the cross-correlation analysis on subsections of the spectrum. In the case of these observations, rms noise considerations limit the useful spectral range over which the analysis can be applied to $> 3 \text{ km s}^{-1}$. Thus, to describe the magnetic field changes over the maser spectrum, cross-correlation was done in the interval $[(V_i - 1.5), (V_i + 1.5)] \text{ km s}^{-1}$, with V_i taken along the spectrum at steps of 3 channel widths. Examples of such 'running' cross-correlation are shown in Fig. 1 with only magnetic field values plotted that had $> 5\sigma$ significance. Special care has to be taken with velocity intervals which are dominated by the wings of a bright emission peak. In this case, remaining gain errors between RCP and LCP could create a spurious Zeeman detection. Although a test with varying gain factors indicates that the 'running' cross-correlation is robust against cases with a uniform gain error across the spectrum, small baseline variations can still cause errors. Thus, only Zeeman determinations in velocity intervals that included a separate maser feature (i.e. a local flux maximum) in the inner 80% of the interval were taken to be significant. It should be noted that, as the 'running' cross-correlation effectively convolves the spectra down to a 3 km s^{-1} spectral resolution, apparent gradual magnetic field variations are introduced when spectral features with a different field strength are blended together. This gradual magnetic field change between the maser features is thus not necessarily physically the case in the maser region.

Although the analysis was performed using the cross-correlation method, the circular polarization pattern as expected from Zeeman splitting was detected for several of the least complex sources. The magnitude of the circular polarization was $\sim 0.2\%$. Fig. 2 shows an example of two sources. The case of Cepheus A illustrates the problem with determining magnetic fields from the circular polarization produced by such a complex maser. Although the structure of the Cepheus A circular polarization is similar to the total power derivative, it is extremely difficult to properly distinguish the individual features.

2.4. Error analysis

Small amplitude non-Gaussian effects on the spectral baselines can introduce an additional uncertainty in the Zeeman splitting determination. To estimate this effect, Monte-Carlo modeling

¹ The 100-m telescope at Effelsberg is operated by the Max-Planck-Institut für Radioastronomie (MPIfR) on behalf of the Max-Planck-Gesellschaft (MPG)

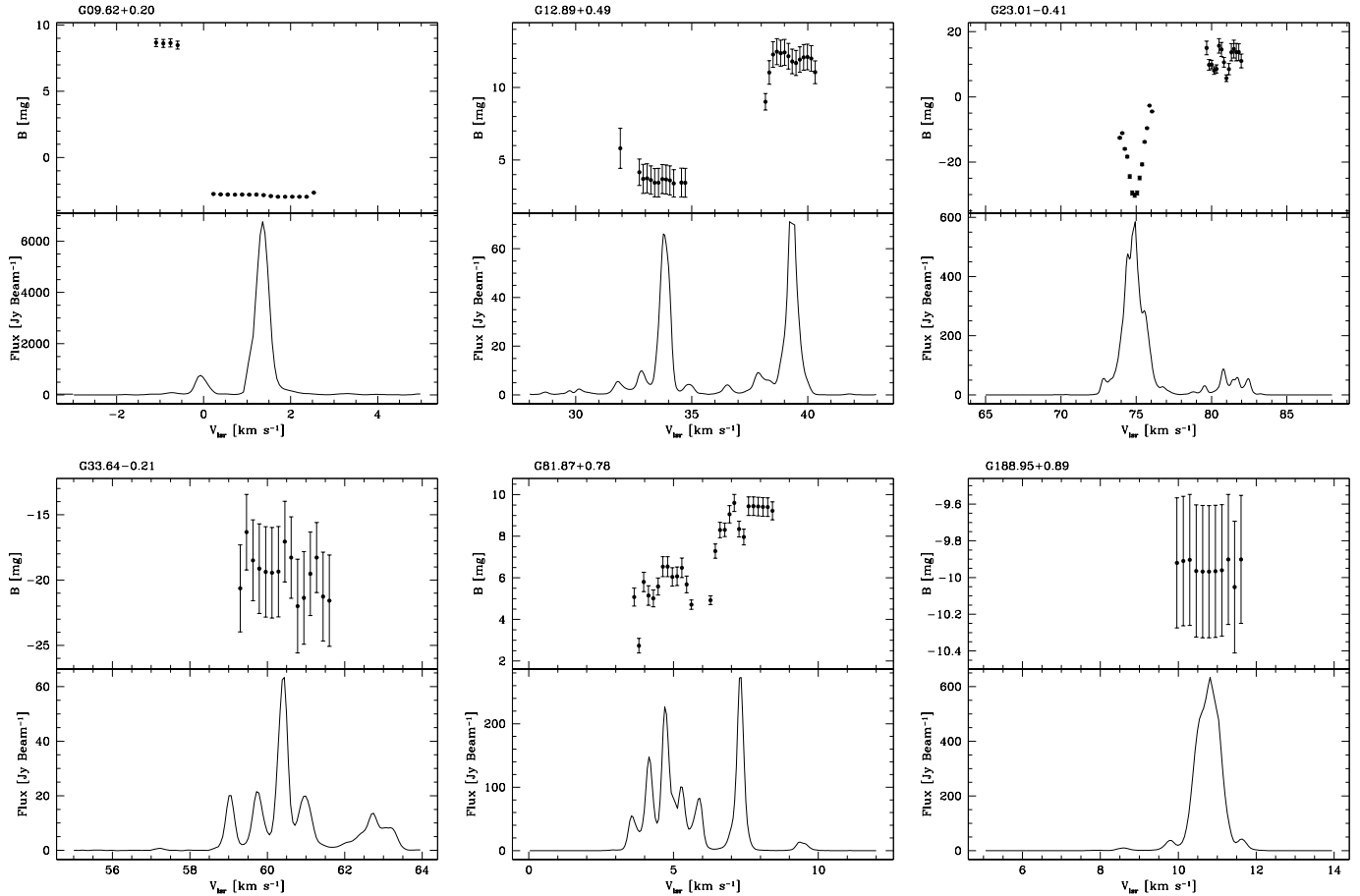


Fig. 1. Total intensity spectra (bottom) and magnetic field strengths (top) for six sources of our sample. The magnetic field strength is determined from the measured Zeeman splitting using the current best value for the 6.7 GHz methanol maser splitting coefficient. The Zeeman splitting is derived using the ‘running’ cross-correlation method (see text).

was performed using artificially generated maser spectra with actual baselines taken from emission free spectral regions for each of the sources of the sample. It was found that typically the rms from the cross-correlation Zeeman splitting calculations need to be increased by $\sim 15\%$ to accommodate this effect. This additional source of error has been included in the errors quoted below.

2.5. Beam Squint

The effect of a slight difference in the pointing center between the RCP and LCP, as a result of both feeds being off-axis, is called beam squint (e.g. Heiles, 1996). Beam squint can mimic the effect of Zeeman splitting when a velocity gradient is present across extended emission of a spectral line, as the RCP and LCP telescope beam will then be probing gas at a slightly different velocity. This severely complicates the Zeeman splitting observations of extended thermal line emission and needs significant additional effort by rotating the feeds during the observations.

However, typically, individual maser features are not very extended. Minier et al. (2002) found that the majority of the methanol masers consist of a compact core with a diffuse halo structure of up to a few hundred AU, corresponding to up to 100 mas. Even for the most extended sources, such as W3(OH), where methanol maser emission extends over sev-

eral arcseconds, the bulk of the maser flux which dominates the Zeeman splitting determination, comes from a region smaller than 100 mas. The pointing difference between the Effelsberg RCP and LCP receivers are $\lesssim 1''$ (e.g. Fiebig, 1990). The effect of beam squint will be most severe when the velocity gradient exists in the direction of the beam off-set. Thus, during longer observation scans, any artificial circular polarization signature will be quenched when the feeds rotate under the source. However, as the observation scans were occasionally as short as a few minutes, it was determined to what level beam squint could contribute to the observed Zeeman splitting. Assuming the worst case, a velocity gradient across the maser in the direction of the RCP-LCP beam off-set, a broad maser spectrum of $\sim 5 \text{ km s}^{-1}$ and a maser extension of 100 mas, the contribution of the beam squint to the Zeeman splitting is found to be less than 0.002 m s^{-1} , corresponding to 0.04 mG. The beam squint circular polarization signature and the regular maser Zeeman splitting only becomes similar if the maser would extend over more than $5''$. However, when an extended maser region consists of individual compact maser features that dominate the spectrum, the beam squint effect is negligible. It can thus be concluded that the velocity splitting between RCP and LCP measured for the 6.7 GHz methanol maser sources is not due to beam squint.

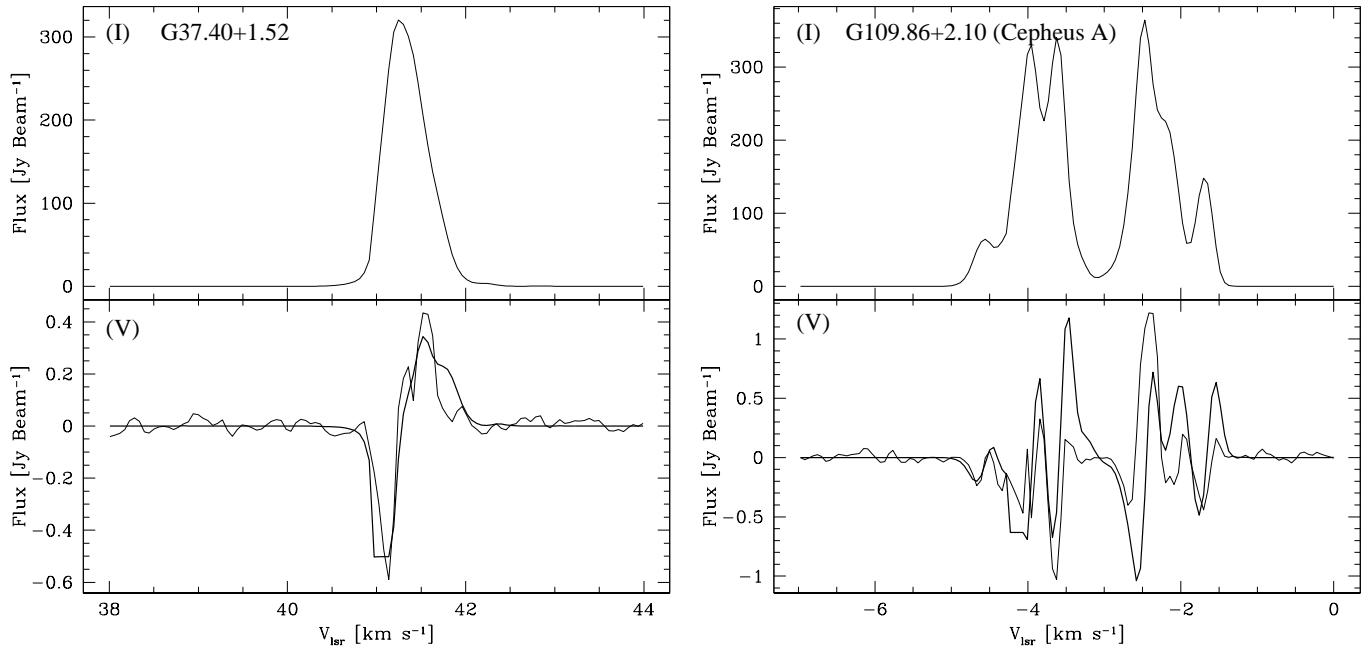


Fig. 2. Total intensity and circular polarization spectrum for G37.40+1.52 (left) and G109.86+2.10 (Cepheus A; right). The thick solid line in the bottom panel is best fit fractional total power derivative to the circular polarization spectrum

3. Methanol maser circular polarization

3.1. Zeeman splitting

The methanol molecule is non-paramagnetic and as a result the Zeeman splitting under the influence of a magnetic field is extremely small. The split energy, ΔE_Z , of an energy level under the influence of a magnetic field, B , is described by $\Delta E_Z = 10^4 g \mu_N M_J B$. Here M_J denotes the magnetic quantum number for the rotational transition with the rotational quantum number J , B is the magnetic field strength in Gauss, μ_N is the nuclear magneton and g is the Landé g -factor, which thus determines the magnitude of the Zeeman effect. This factor was investigated many years ago by Jen (1951), who found empirically that it is probably an average of the true g -factor of several interacting states and can be described by the equation:

$$g = 0.078 + 1.88/[J(J+1)]. \quad (1)$$

This is based on laboratory measurements using 25 GHz methanol masers lines and as a result one has to be careful applying these results to the 6.7 or 12.2 GHz masers. However, until further laboratory studies, this remains the best estimate and implies, for the 6.7 GHz methanol transition, a Zeeman splitting coefficient of $0.049 \text{ km s}^{-1} \text{ G}^{-1}$. It is difficult to properly judge the uncertainty in this value. Conservatively, one expects that magnetic field strengths determined using this value are within $\sim 25\%$ of the true value.

3.2. Non-Zeeman effects

There are several, non-instrumental, effects other than Zeeman splitting that might cause circular polarization of the maser line. One possibility is a rotation of the axis of symmetry for the molecular quantum states. This can occur when, as the maser sat-

urates, the rate for maser stimulated emission R becomes larger than the Zeeman frequency shift $g\Omega$. While $g\Omega \gg R$, the magnetic field direction is the quantization axis. Then, when R becomes smaller than $g\Omega$, the molecules interact more strongly with the radiation field than with the magnetic field and the quantization axis changes towards the maser propagation direction. From the Zeeman splitting coefficient derived above, $g\Omega \approx 22B[\text{mG}] \text{ s}^{-1}$ for the 6.7 GHz methanol maser. The rate for stimulated emission can be estimated using:

$$R \approx AkT_b \Delta\Omega / 4\pi h\nu. \quad (2)$$

Here A is the Einstein coefficient for the maser transition, which is equal to $0.1532 \times 10^{-8} \text{ s}^{-1}$ (Cragg et al., 1993), and k and h are the Boltzmann and Planck constants respectively. The maser frequency is denoted by ν , and T_b and $\Delta\Omega$ are the maser brightness temperature and beaming solid angle. Observations indicate that $T_b \leq 10^{12} \text{ K}$ (Minier et al., 2002), but $\Delta\Omega$ is somewhat harder to estimate and decreases rapidly with increasing maser saturation level. For a typical maser beaming angle of $\Delta\Omega \approx 10^{-2}$, the maser stimulated emission $R \leq 4 \text{ s}^{-1}$. Thus, even in the most saturated case $g\Omega \gg R$ when the magnetic field strength is $\gtrsim 1 \text{ mG}$. A change of quantization axis is thus unable to explain the observed circular polarization.

Alternatively, Wiebe & Watson (1998) have shown that the propagation of strong linear polarization can cause circular polarization when the direction of the magnetic field changes significantly along the maser propagation direction. For a smooth change of magnetic field direction of $\sim 1 \text{ rad}$ along the maser, the fractional circular polarization caused by this effect is approximately $m_l^2/4$, where m_l is the fractional linear polarization. For the typical 6.7 GHz methanol maser linear polarization fraction of $2 - 3\%$, this implies that the generated circular polarization is only $\sim 0.02\%$, which is less than 10% of the observed circular polarization. And, the fairly constant linear polarization vectors

observed at high-resolution (e.g. Vlemmings et al., 2006b), indicate that the magnetic field rotation along the maser path length is likely much smaller than 1 rad, making the propagation of linear polarization an unlikely source of the methanol maser circular polarization.

Finally, a velocity gradient in intrinsic circular polarization (i.e. not caused by the magnetic field) could mimic the effect of Zeeman splitting. However, as in a maser the stimulated emission quickly dominates the intrinsic emission, any intrinsic circular polarization quickly becomes negligible. This is described in more detail in e.g. Elitzur (1998).

4. Results

The results of the Zeeman splitting analysis using the RCP-LCP cross-correlation method are presented in Table 1. The table lists the source name, position, central V_{LSR} velocity, peak and integrated flux and the measured Zeeman splitting ΔV_z . As described in § 2.3, this value corresponds to the flux averaged Zeeman splitting of the entire maser spectrum. In the final column it lists the strength of the magnetic field component along the line-of-sight (B_{\parallel}) determined using the current best value of the 6.7 GHz methanol maser Zeeman splitting coefficient as discussed in § 3. Throughout the paper, the quoted magnetic field strength will correspond to this value. Should in the future a better value of the Zeeman coefficient be determined then all magnetic field values need to be adjusted correspondingly.

Fig. 1 shows six methanol maser spectra and corresponding magnetic fields derived using the running cross-correlation method described in § 2.3. The figure shows that for a number of the sources, the magnetic field changes across the maser. For those sources, Table 1 also lists separately the magnetic field derived for sub-sections of the spectrum. Total intensity spectra and magnetic field strengths for all the sources in the sample with a significant Zeeman detection are presented in the Online material as Figs. 6 and 7. Online Fig. 8 shows the total intensity spectra for the sources without Zeeman detection.

4.1. Individual Sources

A number of the maser sources from the sample have been observed at high angular resolution, providing information on the morphology of the methanol maser region. Additionally, several sources have been the target of magnetic field measurements using mainly OH and/or H₂O maser polarization observations. Sources for which high-resolution 6.7 GHz observations and/or additional magnetic field measurements are available are discussed here in detail.

4.1.1. 09.62+0.20

The 6.7 and 12.2 GHz methanol masers associated with the high-mass star formation complex G09.62+0.20 undergo periodic flares with a period of 244 days, making these the first reported incidence of periodic variations in a high-mass star-forming region (Goedhart et al., 2003, 2004). The origin of the periodic behavior, however, is still unclear. The 6.7 GHz methanol masers have been mapped with the ATCA by Phillips et al. (1998), and the strongest features are shown to be associated with the hypercompact HII region labeled E by Garay et al. (1993). This region also hosts OH masers for which Zeeman splitting observations indicates a magnetic field strength of ~ 5 mG (Fish et al., 2005). As seen in Fig. 1, the magnetic field determined from the 6.7 GHz

methanol maser Zeeman splitting reverses direction between the second-strongest maser feature at $V_{\text{LSR}} = -0.1$ km s⁻¹ ($B_{\parallel} = 8.6$ mG) and the strongest feature at 1.2 km s⁻¹ ($B_{\parallel} = -2.96$ mG), even though the ATCA image shows that the features are located within ~ 100 mas of each other. The periodicity of the flaring of both maser features is the same, with the weaker of the two features flaring with a ~ 1 month delay. There is an intriguing possibility that the maser flaring and time delay is the result of a periodic change in the magnetic field orientation due to a form of magnetic beaming (e.g. Gray & Field, 1994). However, this hypothesis needs to be tested by magnetic field monitoring observations and improved maser modeling.

4.1.2. 12.89+0.49, IRAS 18089-1732

This young massive star-forming region contains methanol, H₂O and OH maser emission as well as a weak hypercompact HII region. The 6.7 GHz methanol masers have been mapped with the ATCA and consist of two regions separated by $\sim 1.5''$ (Walsh et al., 1997). The strong maser feature at $V_{\text{LSR}} = 33.6$ km s⁻¹, which shows the smallest Zeeman splitting ($B_{\parallel} = 4$ mG) is located closest to the sub-millimeter continuum peak imaged by Beuther et al. (e.g. 2005) at high-resolution with the submillimeter array (SMA). The higher velocity features, with $B_{\parallel} = 12$ mG, are located in the direction of the North-South molecular outflow found in the same SMA observations. The OH masers on the other hand, are located in the direction of extended molecular emission in the East-West direction, which shows indications of a rotation signature perpendicular to the outflow (Beuther et al., 2005; Beuther & Walsh, 2008). The magnetic field measured from OH maser Zeeman splitting is $B = 3.93$ mG (Ruiz-Velasco et al., 2006).

4.1.3. 23.01-0.41

The Zeeman splitting for this source, and consequently the magnetic field, shows a very strong negative magnetic field for the brightest maser peak at $V_{\text{LSR}} = 74.9$ km s⁻¹ ($B_{\parallel} = -30.3$ mG), while the other maser features have a positive field direction with a strength of $B_{\parallel} \approx 14$ mG. In Fig. 1, this results in a dip towards an increasingly negative magnetic field across the maser, because, as described in § 2.3, the running average calculates the Zeeman splitting over a 3 km s⁻¹ interval. Szymczak & Gérard (2004) find a 1667 MHz OH maser feature with a magnetic field strength of $B = -0.2$ mG at $V_{\text{LSR}} = 74.31$ km s⁻¹. Unfortunately, no high resolution maps are available to check the morphology of the maser source.

4.1.4. 31.28+0.06, IRAS 18456-0129

The largest Zeeman splitting was measured for the masers of the UC HII region G31.28+006, which is part of the giant HII region W43, and correspond to $B_{\parallel} = 42$ mG. The 6.7 GHz methanol masers were observed with the European VLBI Network (EVN) and reveal a complex distribution over $\sim 400 \times 400$ mas (Minier et al., 2000). No other maser polarization observations are found in the literature.

4.1.5. 33.64-0.21

As seen in Fig. 1, the magnetic field of this source is stable over the entire velocity range with a flux averaged strength of $B_{\parallel} = -18$ mG. The only other magnetic field measure-

Table 1. Zeeman splitting results

Source		α_{J2000} <i>hh mm ss</i>	δ_{J2000} <i>° ' "</i>	V_{LSR} km s^{-1}	Peak Flux (Jy/beam)	Int. Flux (Jy/beam)	ΔV_z m s^{-1}	$ B $ (mG)
09.62+0.20 ^a		18 06 14.66	-20 31 31.60	1.0	6757	3091	-0.137 ± 0.002	-2.80 ± 0.04
				-0.1 ^b			0.42 ± 0.02	8.6 ± 0.4
12.89+0.49 ^a	IRAS 18089-1732	18 11 51.46	-17 31 28.84	1.2 ^b	71	105	-0.145 ± 0.002	-2.96 ± 0.04
				39.3			0.41 ± 0.03	8.4 ± 0.7
				34.8 ^b			0.18 ± 0.05	4 ± 1
23.01-0.41 ^a		18 34 40.37	-09 00 38.30	39.2 ^b	585	1016	0.59 ± 0.05	12 ± 1
				74.8			-1.49 ± 0.03	-30.3 ± 0.7
				74.9 ^b			-1.49 ± 0.02	-30.3 ± 0.4
				81.0 ^b			0.7 ± 0.1	14 ± 2
25.71+0.04		18 38 03.10	-06 24 32.00	95.6	590	591	< 0.06	< 1.2
25.83-0.18		18 39 04.70	-06 24 17.00	90.7	69	84	0.99 ± 0.20	20 ± 4
28.15+0.00		18 42 41.00	-04 15 21.00	101.3	30	24	< 1.8	< 37
31.28+0.06	IRAS 18456-0129	18 48 12.38	-01 26 22.60	110.4	74	174	2.06 ± 0.26	42 ± 5
32.03+0.06	IRAS 18470-0050	18 49 37.04	-00 46 50.10	98.7	69	81	< 0.51	< 11
33.64-0.21		18 53 28.70	+00 31 58.00	58.6	63	54	-0.89 ± 0.17	-18 ± 3
35.20-0.74	IRAS 18556+0136	18 58 12.98	+01 40 37.50	30.5	169	167	0.81 ± 0.04	16.5 ± 0.7
35.20-1.74	W48	19 01 45.60	+01 13 28.00	41.5	476	643	0.32 ± 0.02	6.4 ± 0.3
37.40+1.52	IRAS 18517+0437	18 54 13.80	+04 41 32.00	41.0	320	193	0.75 ± 0.02	15.4 ± 0.4
43.80-0.13	W49N	19 11 55.10	+09 36 00.00	40.0	35	81	< 1.9	< 39
49.49-0.39	W51-e1/e2	19 23 44.50	+14 30 31.00	59.0	1029	885	0.72 ± 0.04	14.7 ± 0.8
69.52-0.97	ON1	20 10 09.07	+31 31 34.40	11.6	96	45	< 0.2	< 4.1
78.10+3.64	IRAS 20126+4104	20 14 26.04	+41 13 33.39	-6.1	60	77	< 0.8	< 17
81.87+0.78 ^a	W75N	20 38 36.80	+42 37 59.00	5.0	273	317	0.40 ± 0.02	8.2 ± 0.3
				5.0 ^b			0.28 ± 0.02	5.7 ± 0.4
				7.3 ^b			0.46 ± 0.02	9.4 ± 0.4
109.86+2.10	Cepheus A	22 56 18.09	+62 01 49.45	-4.2	364	484	0.39 ± 0.01	8.1 ± 0.2
111.53+0.76 ^a	NGC 7538	23 13 45.36	+61 28 10.55	-56.1	233	514	0.79 ± 0.03	16.2 ± 0.6
				-58 ^b			0.78 ± 0.04	16.0 ± 0.8
				-56 ^b			0.59 ± 0.02	12.1 ± 0.4
133.94+1.04	W3(OH)	02 27 04.72	+61 52 24.73	-44.0	3705	8198	0.141 ± 0.003	2.87 ± 0.05
173.49+2.42	S231	05 39 13.06	+35 45 51.29	-13.0	52	53	0.95 ± 0.11	19 ± 2
174.19-0.09	AFGL 5142	05 30 42.00	+33 47 14.00	2.1	55	34	< 0.8	< 18
188.95+0.89	IRAS 06058+2138	06 08 53.35	+21 38 28.67	10.9	633	485	-0.49 ± 0.02	-9.9 ± 0.4
192.60-0.05	S255	06 12 54.02	+17 59 23.00	5.0	94	78	0.47 ± 0.05	9.6 ± 0.9

^a Significant magnetic field changes across the maser spectrum.

^b Velocity of the maser feature for which Zeeman splitting was determined separately.

ment for 33.64-0.21 comes from a single 1720 mG OH maser feature at $V_{LSR} = 60.23 \text{ km s}^{-1}$, which has $B = -1 \text{ mG}$ (Szymczak & Gérard, 2004).

4.1.6. 35.20-0.74, IRAS 18556+0136

The methanol masers of the bipolar outflow source G35.20-074N have only recently been mapped using the Japanese VLBI Network (Sugiyama et al., 2007), showing that the brightest features make up two compact regions separated by more than 2'' in a direction perpendicular to the CO outflow, along a putative molecular disc (Dent et al., 1985). The Zeeman splitting observations indicate a stable flux averaged magnetic field strength of $B_{\parallel} = 16.5 \text{ mG}$, which is likely dominated by the strongest maser feature at $V_{LSR} = 28.7 \text{ km s}^{-1}$ in the southern maser cluster. The OH maser polarization of this source has been studied with MERLIN by Hutawarakorn & Cohen (1999), who find that the magnetic field reverses on opposite sides of the disc. The OH maser distribution is thought to lie along the disc, with the southern masers tracing a mean field $B \approx 4 \text{ mG}$ and a northern maser feature having $B = -2.5 \text{ mG}$.

4.1.7. 35.20-1.74, W48

The UC HII region G 35.20-1.74, in the Galactic HII region W48, is believed to be a site of massive star formation and has both OH and methanol masers. EVN observations of the 6.7 GHz methanol maser region shows a ring-like structure of $\sim 200 \times 400 \text{ mas}$ (Minier et al., 2000). Although the spectrum is complex, the Zeeman splitting observations do not show any large variations and yield a flux averaged field strength of $B_{\parallel} = 6.4 \text{ mG}$. The magnetic field at the periphery of the UC HII region has been determined from carbon recombination line observations, which give a field of $B = 2.9 \text{ mG}$ at a hydrogen number density of $n_{\text{H}_2} = 8.5 \cdot 10^6 \text{ cm}^{-3}$ (Roshi et al., 2005).

4.1.8. 49.49-0.39, W51-e1/e2

W51 is one of the most luminous massive star formation complexes of our Galaxy and can be divided in three regions, W51A, W51B and W51C (Carpenter & Sanders, 1998). The maser site G49.49-0.39 is associated with W51A and particularly with W51-e1/e2 (Caswell et al., 1995). OH maser polarization observations reveal a total of 46 Zeeman pairs near e1 and e2, with the region having predominantly a positive magnetic field direction which reverses in the northern part of e1 (Fish & Reid, 2006). W51e2 has two Zeeman pairs that imply a magnetic field of the

order of ~ 20 mG (Argon et al., 2002), with the rest of the OH masers indicating $B \sim 5$ mG. For the 6.7 GHz methanol masers the Zeeman splitting indicates a flux averaged $B_{\parallel} = 14.7$ mG.

4.1.9. 69.52-0.97, ON1

The 6.7 GHz methanol maser emission and polarization was recently mapped with MERLIN by Green et al. (2007). Those observations indicate a tentative first detection of 6.7 GHz methanol maser Zeeman splitting of 9 ± 3 m s $^{-1}$, corresponding to a field strength of -18 mG. This marginal detection could not be confirmed in the observations presented here. However, the Zeeman splitting measured by Green et al. was found on a maser feature that, in lower resolution observations, would be blended both positionally and spectroscopically with the brightest maser. As a result, the flux averaged Zeeman splitting measurement is biased toward a possibly negligible magnetic field of the brightest feature.

4.1.10. 81.87+0.78, W75N

The 6.7 GHz methanol masers of the very active region of massive star formation W75N have been mapped with the EVN (Minier et al., 2000). Their map reveals that the masers make up two distinct regions, an elongated region of ~ 200 mas with $V_{\text{LSR}} < 6$ km s $^{-1}$ and a compact feature ~ 500 mas South-East at $V_{\text{LSR}} = 6.8$ km s $^{-1}$. The observations shown in Fig. 1 highlight the distinct nature of these maser features as the masers in the linearly extended structure have $B_{\parallel} = 5.7$ mG while those in the compact region have $B_{\parallel} = 9.5$ mG. W75N has been the target of numerous OH maser polarization observations indicating another possible disc related field reversal and typical magnetic field strengths of $|B| \approx 5 - 7$ mG (e.g. Hutawarakorn et al., 2002; Slysh et al., 2002). Magnetic field measurements during a OH maser flare in W75N reveal the strongest OH maser magnetic field $B = 40$ mG to date (Slysh & Migenes, 2006).

4.1.11. 109.86+2.10, Cepheus A

The masers of the Cepheus A massive star formation region has been studied in great detail (e.g. Vlemmings et al., 2006a, and references therein). The 6.7 GHz methanol maser distribution has been mapped with the Japanese VLBI Network (Sugiyama et al., 2007) and the EVN (Torstensson et al., in prep.). These observations show that the masers are found in an elongated structure of ~ 1500 mas across Cepheus A HW2. The measured methanol maser magnetic field is stable at $B_{\parallel} = 8.1$ mG.

Cepheus A is the source in the sample for which the most magnetic field measurements at different hydrogen density are available. Fig. 3 presents an overview of all these measurements. It seems clear that the magnetic field strength B in Cepheus A has a power-law dependence on the hydrogen number density n_{H_2} , with the best-fit giving $B \propto n^{-0.47 \pm 0.08}$. This is consistent with the empirical relation $B \propto n^{-0.47}$ from low-density molecular cloud Zeeman observations by Crutcher (1999). Of course, one has to be cautious when relating the maser observations with the other Zeeman splitting results and the dust polarization observations at very different scales. Additionally, the methanol and H $_2$ O maser magnetic field strengths depend on an assumption with regard to the angle between the maser propagation direction and the magnetic field and their number density has to be determined using maser excitation models.

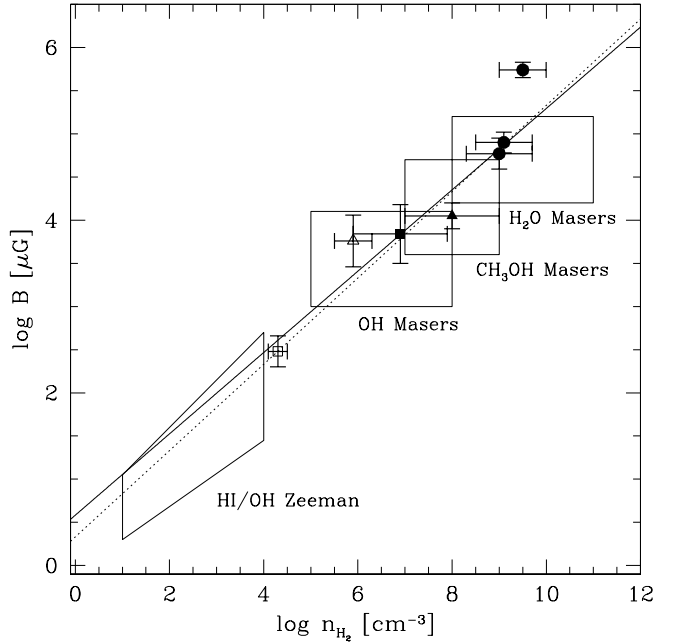


Fig. 3. Magnetic field strength B in the massive star forming region Cepheus A measured from Zeeman measurements as a function of n_{H_2} , the number density of neutral hydrogen. The solid triangle indicates the methanol maser measurement from the Effelsberg observations, the number density is taken to be in the range typical of 6.7 GHz methanol masers (Cragg et al., 2005), but cannot be determined precisely without observations of additional transition lines. Also indicated are the H $_2$ O maser measurements (solid dots; Vlemmings et al., 2006a), average OH maser measurement (solid square; Bartkiewicz et al., 2005), NH $_3$ measurement (open square; Garay et al., 1996) and recent dust polarization measurement (open triangle; Curran & Chrysostomou, 2007). The error bars on the density of these data are taken from the respective publications. The solid line is the theoretical relation $B \propto n^{0.5}$ fixed to the OH maser measurement. The dashed line is the error weighted best fit line to the presented measurements (the individual H $_2$ O maser measurements were averaged). Additionally, the boxes indicate the range of literature values for HI/non-masing OH, OH maser, methanol maser (this paper) and H $_2$ O maser Zeeman splitting observations for other massive star formation regions.

4.1.12. 111.53+0.76, NGC 7538

The methanol masers of NGC 7538 have been proposed to trace a disk around a high-mass protostar (Pestalozzi et al., 2004), however, this interpretation has been questioned by De Buizer & Minier (2005) who find that the maser might be related to an outflow. The observations presented here indicate a flux averaged magnetic field $B_{\parallel} = 16.2$ mG. The 'running' cross-correlation however, reveals a more complex picture. The spectrum is made up of several strong maser features with apparently different magnetic field strengths. The strongest magnetic field ~ 16 mG is measured on the maser feature at $V_{\text{LSR}} = -58$ km s $^{-1}$, while ~ 12 mG is found for the maser at $V_{\text{LSR}} = -56$ km s $^{-1}$. In both cases the 'running' cross-correlation derived magnetic field is somewhat suppressed as the masers between $V_{\text{LSR}} = -58$ and -56 km s $^{-1}$ have a field of only a

few mG. Meanwhile, no significant magnetic field is detected in the masers near $V_{\text{LSR}} = -61 \text{ km s}^{-1}$, implying a field strength $B_{\parallel} \lesssim 5 \text{ mG}$. The flux averaged magnetic field is marginally larger than the field determined using the 'running' cross-correlation for individual maser features. This is due to the fact that, in determining the flux averaged field strength, strong fields, which have nevertheless $< 5\sigma$ significance in the smaller 3 km s^{-1} intervals used for the 'running' cross-correlation, still contribute. OH maser measurements indicate the region undergoes a field reversal and has $|B| = 1 \text{ mG}$ (Fish & Reid, 2006).

4.1.13. 133.94+1.04, W3(OH)

Linear polarization of the 6.7 GHz methanol masers of W3(OH) is described in Vlemmings et al. (2006b), who also give a compilation of previous OH maser magnetic field strength measurements. The polarization observations show that the magnetic field traces the extended methanol filament but has a more complex structure in the dominating compact region described in Harvey-Smith & Cohen (2006). The Zeeman splitting presented here corresponds to a flux averaged magnetic field strength of $B_{\parallel} = 2.87 \text{ mG}$. However, due to the rich spectrum and large extent of W3(OH) a direct comparison with other Zeeman splitting measurements is impossible and would need high resolution observations.

5. Discussion

5.1. Magnetic field strength

Significant Zeeman splitting was detected for 17 out of 24 sources and indicates an absolute magnetic field strength component $|B_{\parallel}|$ along the maser propagation direction between 2.8 and 42 mG. There are several effects that bias the observed field strength towards higher or lower values. As is the case for H_2O masers, low spatial resolution observations, velocity gradients across the maser and increased maser saturation tend to cause an underestimate of the magnetic field strength (Sarma et al., 2001; Vlemmings, 2006). As discussed above, beam squint can create a false Zeeman splitting signature, however, for milliarcsecond-scale masers this is unlikely to contribute more than $\sim 0.04 \text{ mG}$. Finally, the Zeeman coefficient which is used to determine the magnetic field is uncertain, as is described in § 3, which leads to a systematic bias in the magnetic field. Thus the uncertainty in the measured absolute magnetic field strength will be substantial, with most of the described effects biasing it towards a value that is lower than the actual field strength. Weighing the field strength by measurement significance, the average magnetic field $\langle B_{\parallel, \text{meth}} \rangle = 12 \text{ mG}$. This needs to be corrected for a random angle between magnetic field and the line-of-sight, which implies for the absolute field strength $|B| = 2\langle B_{\parallel} \rangle$ (e.g. Crutcher, 1999). This gives $|B_{\text{meth}}| = 23 \pm 6 \text{ mG}$. The error on the absolute field strength is dominated by the estimated uncertainty in the Zeeman coefficient. This field strength is larger than that found in the OH maser regions, with the average OH maser determined field strength being $\sim 4 \text{ mG}$ (Fish & Reid, 2006).

The dynamical importance of the magnetic field can be quantified by defining a critical magnetic field strength $B_{\text{crit}} = (8\pi\rho v^2)^{1/2}$ for which the dynamic and magnetic pressure are equal. Here ρ and v are the density and velocity of the maser medium respectively. Cragg et al. (2005) find that the current observational limits suggest that the majority of the 6.7 GHz maser sources occur near the high-density limit of the maser range ($n_{\text{H}_2} = 10^7 - 10^9 \text{ cm}^{-3}$), with a typical value of $n_{\text{H}_2} =$

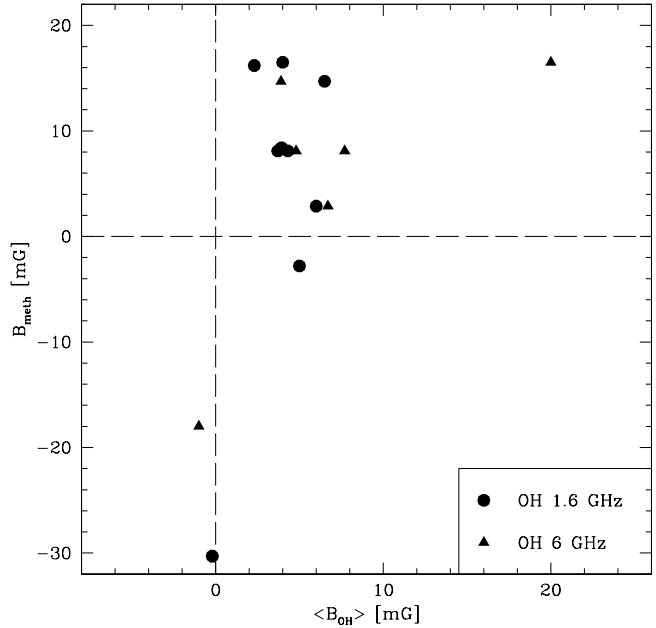


Fig. 4. Measured flux averaged 6.7 GHz methanol maser magnetic field strength vs. average 1.6 and 6 GHz OH maser magnetic field strengths for those sources where both are available. Most literature values were taken from the compilation of molecular cloud magnetic field measurements by Han & Zhang (2007).

10^8 cm^{-3} . Taking this density and a typical gas velocity of $\lesssim 5 \text{ km s}^{-1}$ from proper motion measurements (e.g. Xu et al., 2006), $B_{\text{crit}} \approx 12 \text{ mG}$. The measured magnetic field values are thus comparable to B_{crit} and hence dynamically important.

5.2. Comparison with OH masers

Theoretical modeling indicates that, given sufficient abundance, both 1.6 and 6 GHz OH masers as well as the methanol masers can be pumped simultaneously (Cragg et al., 2002). However, observations have shown that, although they are closely associated, co-propagation between OH and methanol masers is rare (e.g. Etoaka et al., 2005). Still, as the masers are closely related, one might expect a relation between the OH magnetic field strengths and those derived from the methanol masers. As seen in Fig. 4, no clear relation is found for those sources which have magnetic field strength measurements from both maser species. This is likely due to the fact that the flux averaged methanol maser magnetic field strengths cannot be easily related to the OH maser measurements often performed at much higher resolution.

Fig. 4 does, however, show that the magnetic field directions determined from methanol and OH masers are fully consistent. As discussed for some of the individual sources, this even holds for regions where the OH masers show a magnetic field reversal. This implies that the magnetic field orientation derived from the methanol maser regions, as that from OH masers, could be indicative of the Galactic magnetic field. This is illustrated in Fig. 5, although a much larger number of measurements as well as accurate distances to the star-forming regions would be needed. Since several efforts are underway to determine accu-

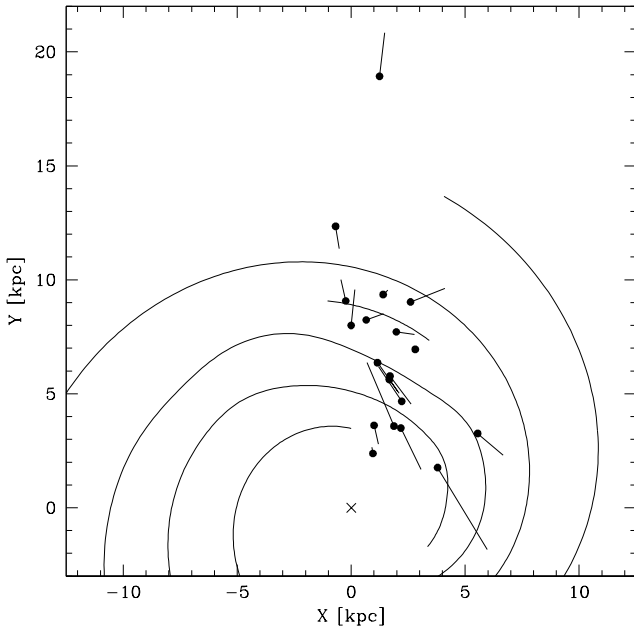


Fig. 5. Magnetic field direction and strength along the line-of-sight derived from the methanol maser Zeeman splitting observations presented in this paper projected onto the Galactic plane. The solid dots are the observed star-forming region with kinematic distances from Pestalozzi et al. (2005). These are known to be highly uncertain. The length of the vectors is scaled with B_{\parallel} . The approximate location of the spiral arms is indicated as taken from Taylor & Cordes (1993).

rate distances to methanol maser regions (e.g Xu et al., 2006), methanol maser Zeeman splitting measurements will provide an important opportunity to study the Galactic magnetic field (e.g. Han & Zhang, 2007).

5.3. The magnetic field vs. density relation

Fig. 3 shows the B -field measurements of both maser and non-maser Zeeman observations as a function of hydrogen number density. The figure seems to indicate that the B -field follows the $B \propto n^{0.5}$ density scaling law discussed in Mouschovias & Ciolek (e.g 1999) over an enormous range of densities. This makes the maser measurements consistent with low-density molecular cloud measurements (Crutcher, 1999), implying that the magnetic field remains partly coupled to the gas up to the highest number densities. However, some care has to be taken in interpreting this relation, as for instance the shock excited masers are short-lived (H_2O masers have a typical lifetime $\tau_m \sim 10^8$ s) compared to the typical ambipolar diffusion time-scale at the highest densities ($\tau_d \sim 10^9$ s). This suggests that in the non-masing gas of similar densities, magnetic field strengths are likely lower due to ambipolar diffusion. Still, the maser magnetic field measurements strongly imply a dynamical importance of magnetic fields during the high-mass star formation process, with the methanol maser observations presented here filling the gap between the OH and H_2O maser observations.

6. Concluding remarks

This paper presents the first significant Zeeman splitting measurements obtained on the 6.7 GHz methanol maser. As this highly abundant maser uniquely pinpoints massive star formation, a detection of the Zeeman splitting gives the opportunity to measure the magnetic field in a large number of high-mass star-forming regions at densities of $n_{\text{H}_2} \approx 10^8 \text{ cm}^{-3}$. The average line-of-sight magnetic field in the methanol maser region $\langle B_{\parallel, \text{meth}} \rangle = 12 \text{ mG}$, although this depends on the exact Zeeman coefficient used to calculate the field strength as discussed in § 3. A statistical correction for a randomly oriented magnetic field gives $|B_{\text{meth}}| = 23 \text{ mG}$. This indicates that the magnetic field is dynamically important. The 100-m Effelsberg telescope observations presented here, detected significant magnetic fields in 70% of the sources with peak fluxes down to $\sim 50 \text{ Jy}$. Thus, with additional observations it will be possible to construct a catalogue of magnetic field measurements for over 100 high-mass star-forming regions giving unique insight in Galactic magnetic fields.

acknowledgments: WV thanks A.Kraus for his help setting up the Effelsberg observations, S.Goedhart for making available her most recent G09.62+0.20 monitoring results and V.Migenes and V.Slysh for providing details on the IRAS 18089-1732 OH maser observations. WV also thanks the referee for comments that have greatly improved the paper.

References

- Argon, A. L., Reid, M. J., & Menten, K. M. 2002, in IAU Symposium, Vol. 206, Cosmic Masers: From Proto-Stars to Black Holes, ed. V. Migenes & M. J. Reid, 367
- Bartkiewicz, A., Szymczak, M., Cohen, R. J., & Richards, A. M. S. 2005, MNRAS, 361, 623
- Beuther, H., Zhang, Q., Sridharan, T. K., & Chen, Y. 2005, ApJ, 628, 800
- Beuther, H., & Walsh, A. J. 2008, ApJ, 673, L55
- Carpenter, J. M. & Sanders, D. B. 1998, AJ, 116, 1856
- Caswell, J. L., Vaile, R. A., & Forster, J. R. 1995, MNRAS, 277, 210
- Cragg, D. M., Mikhtiev M. A., Bettens, R. P. A., et al. 1993, MNRAS, 264, 769
- Cragg, D. M., Sobolev, A. M., & Godfrey, P. D. 2002, MNRAS, 331, 521
- Cragg, D. M., Sobolev, A. M., & Godfrey, P. D. 2005, MNRAS, 360, 533
- Crutcher, R. M. 1999, ApJ, 520, 706
- Curran, R. L. & Chrysostomou, A. 2007, MNRAS, 382, 699
- De Buizer, J. M. & Minier, V. 2005, ApJ, 628, L151
- Dent, W. R. F., Little, L. T., Kaifu, N., Ohishi, M., & Suzuki, S. 1985, A&A, 146, 375
- Elitzur, M. 1998, ApJ, 504, 390
- Ellingsen, S. P. 2002, in IAU Symposium, Vol. 206, Cosmic Masers: From Proto-Stars to Black Holes, ed. V. Migenes & M. J. Reid, 151
- Etoka, S., Cohen, R. J., & Gray, M. D. 2005, MNRAS, 360, 1162
- Fiebig, D. 1990, PhD thesis, Friedrich-Wilhelms Univ., Bonn, (1990)
- Fish, V. L. & Reid, M. J. 2006, ApJS, 164, 99
- Fish, V. L., Reid, M. J., Argon, A. L., & Zheng, X.-W. 2005, ApJS, 160, 220
- Garay, G., Ramirez, S., Rodriguez, L. F., Curiel, S., & Torrelles, J. M. 1996, ApJ, 459, 193
- Garay, G., Rodriguez, L. F., Moran, J. M., & Churchwell, E. 1993, ApJ, 418, 368
- Goedhart, S., Gaylard, M. J., & van der Walt, D. J. 2003, MNRAS, 339, L33
- Goedhart, S., Gaylard, M. J., & van der Walt, D. J. 2004, MNRAS, 355, 553
- Gray, M. D. & Field, D. 1994, A&A, 292, 693
- Green, J. A., Richards, A. M. S., Vlemmings, W. H. T., Diamond, P., & Cohen, R. J. 2007, MNRAS, 382, 770
- Han, J. L. & Zhang, J. S. 2007, A&A, 464, 609
- Harvey-Smith, L. & Cohen, R. J. 2006, MNRAS, 371, 1550
- Heiles, C. 1996, ApJ, 466, 224
- Hill, T., Burton, M. G., Minier, V., et al. 2005, MNRAS, 363, 405
- Hutawarakorn, B. & Cohen, R. J. 1999, MNRAS, 303, 845
- Hutawarakorn, B., Cohen, R. J., & Brebner, G. C. 2002, MNRAS, 330, 349
- Jen, C. K. 1951, Physical Review, 81, 197
- Krumholz, M. R. & Bonnell, I. A. 2007, ArXiv e-prints, 712
- Minier, V., Booth, R. S., & Conway, J. E. 2000, A&A, 362, 1093
- Minier, V., Booth, R. S., & Conway, J. E. 2002, A&A, 383, 614

- Modjaz, M., Moran, J. M., Kondratko, P. T., & Greenhill, L. J. 2005, *ApJ*, 626, 104
- Mouschovias, T. C. & Ciolek, G. E. 1999, in *NATO ASIC Proc. 540: The Origin of Stars and Planetary Systems*, 305
- Pestalozzi, M. R., Elitzur, M., Conway, J. E., & Booth, R. S. 2004, *ApJ*, 603, L113
- Pestalozzi, M. R., Minier, V., & Booth, R. S. 2005, *A&A*, 432, 737
- Phillips, C. J., Norris, R. P., Ellingsen, S. P., & McCulloch, P. M. 1998, *MNRAS*, 300, 1131
- Roshi, D. A., Goss, W. M., Anantharamaiah, K. R., & Jeyakumar, S. 2005, *ApJ*, 626, 253
- Ruiz-Velasco, A. E., Migenes, V., Slysh, V., & Val'tts, I. E. 2006, in *Revista Mexicana de Astronomia y Astrofisica Conference Series*, Vol. 26, 26
- Sarma, A. P., Troland, T. H., & Romney, J. D. 2001, *ApJ*, 554, L217
- Slysh, V. I. & Migenes, V. 2006, *MNRAS*, 369, 1497
- Slysh, V. I., Migenes, V., Val'tts, I. E., et al. 2002, *ApJ*, 564, 317
- Sobolev, A. M., Cragg, D. M., & Godfrey, P. D. 1997, *A&A*, 324, 211
- Sugiyama, K., Fujisawa, K., Doi, A., et al. 2007, *ArXiv e-prints*, 710
- Szymczak, M. & Gérard, E. 2004, *A&A*, 414, 235
- Taylor, J. H. & Cordes, J. M. 1993, *ApJ*, 411, 674
- Vlemmings, W. H. T. 2006, *A&A*, 445, 1031
- Vlemmings, W. H. T., Bignall, H. E., & Diamond, P. J. 2007, *ApJ*, 656, 198
- Vlemmings, W. H. T., Diamond, P. J., van Langevelde, H. J., & Torrelles, J. M. 2006a, *A&A*, 448, 597
- Vlemmings, W. H. T., Harvey-Smith, L., & Cohen, R. J. 2006b, *MNRAS*, 371, L26
- Walsh, A. J., Hyland, A. R., Robinson, G., & Burton, M. G. 1997, *MNRAS*, 291, 261
- Wiebe, D. S. & Watson, W. D. 1998, *ApJ*, 503, L71
- Xu, Y., Reid, M. J., Zheng, X. W., & Menten, K. M. 2006, *Science*, 311, 54

Online Material

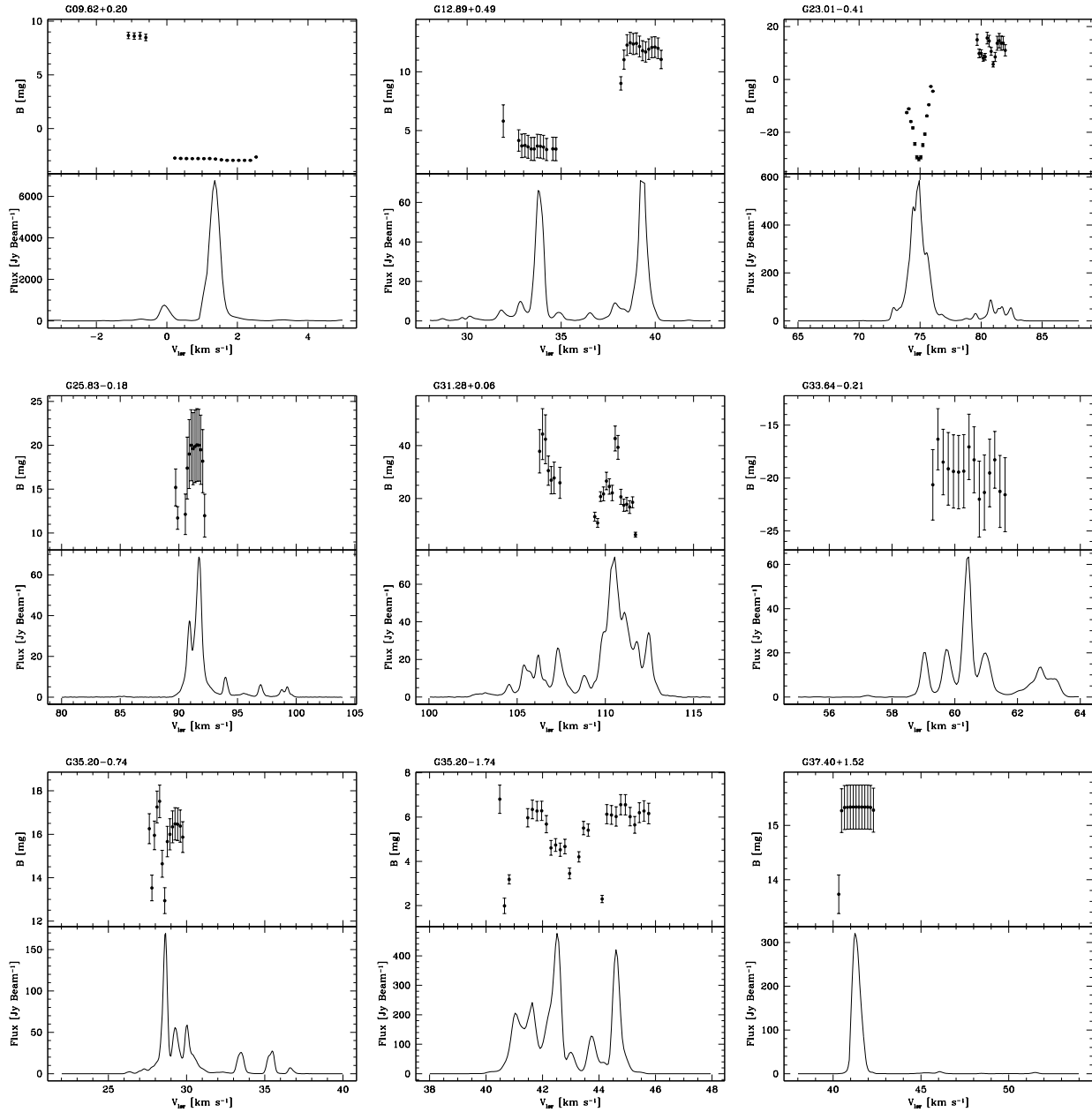


Fig. 6. Total intensity spectra (bottom) and magnetic field strength (top) for all the sources of our sample with significant Zeeman splitting detection. The magnetic field strength is determined from the measured Zeeman splitting using the current best value for the 6.7 GHz methanol maser splitting coefficient. The Zeeman splitting is derived using the ‘running’ cross-correlation method (see § 2.3).

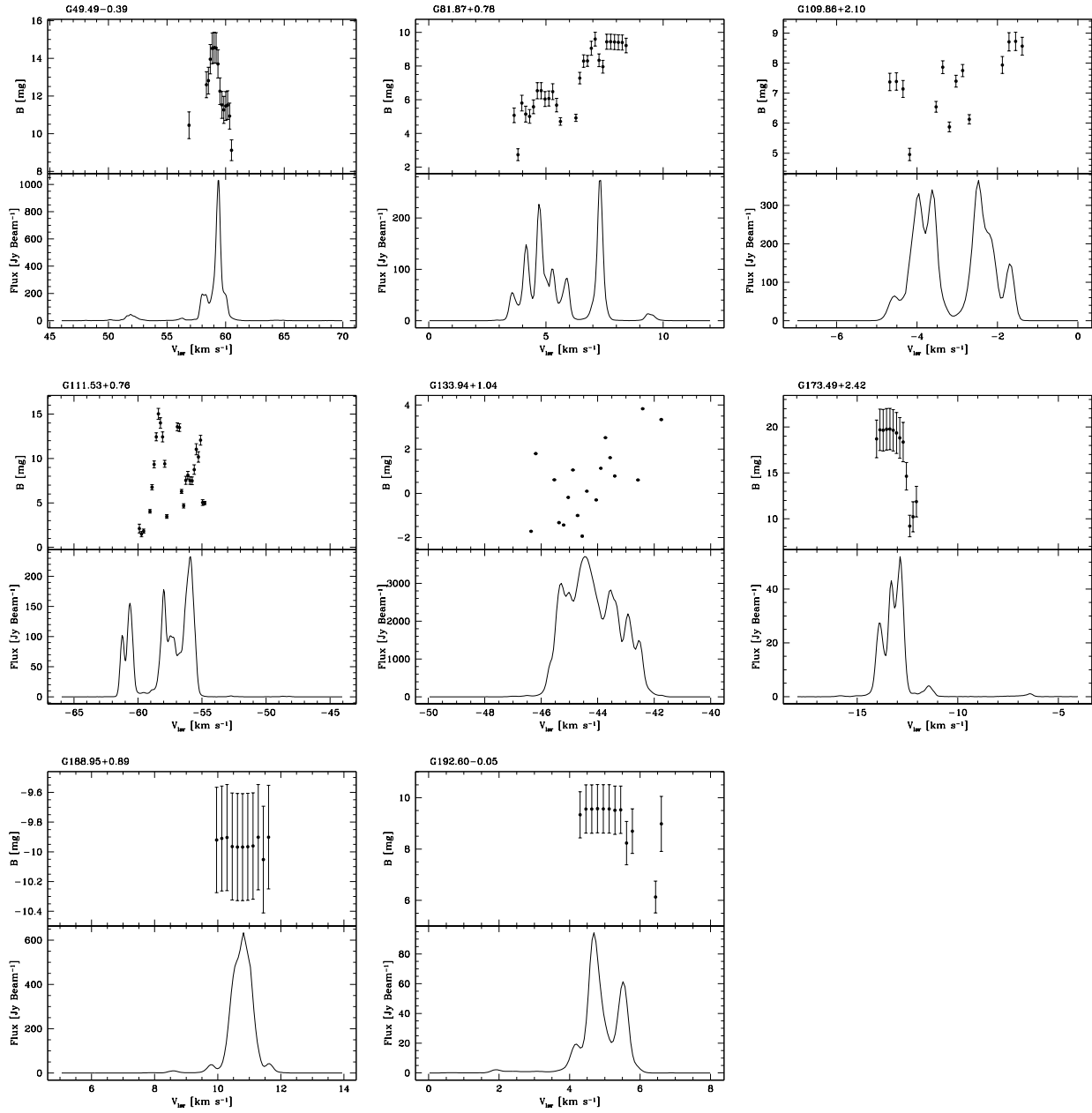


Fig. 7. As Fig. 6.

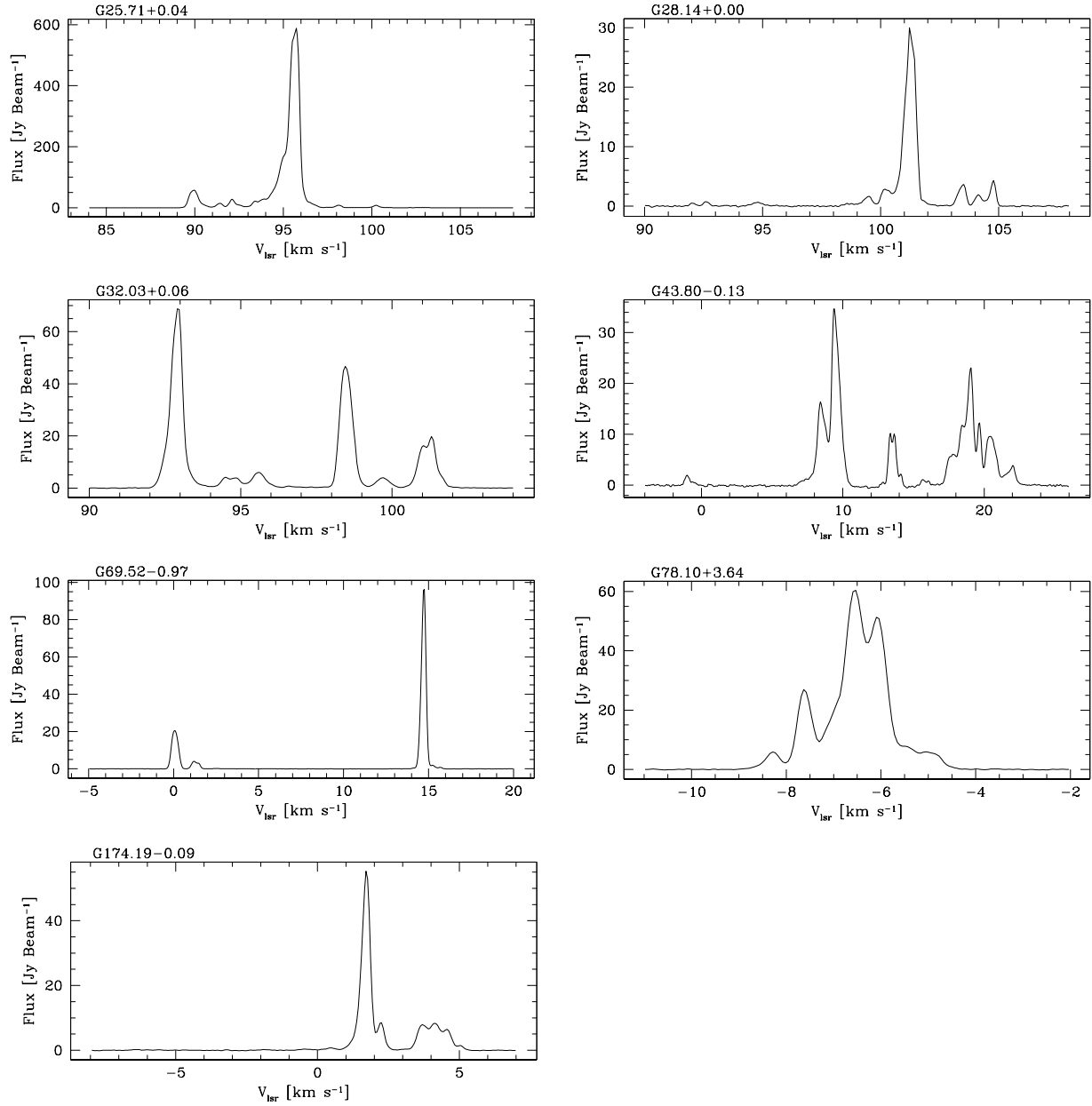


Fig. 8. Total intensity spectra of the sources in our sample for which no significant Zeeman splitting was detected.